Ab Initio Computational Crystallography of 2:1 Clay Minerals: 1. Pyrophyllite-1Tc

Keith Refson*

Rutherford Appleton Laboratory, Chilton, Didcot, Oxfordshire, OX11 0QX, United Kingdom

Sung-Ho Park* and Garrison Sposito

Geochemistry Department, Earth Sciences Division, Lawrence Berkeley National Laboratory, Berkeley, California 94720

Received: March 25, 2003; In Final Form: July 21, 2003

The interpretation of diffraction and spectroscopic data on clay minerals can be facilitated by first-principles quantum mechanical simulations based on density functional theory (DFT), which now has achieved sufficient accuracy to predict crystallographic properties of these minerals without recourse to empirical parametrization. To test the accuracy of DFT for simulating 2:1 clay minerals, we have performed calculations on a related layer aluminosilicate for which high-quality crystallographic data are available, pyrophyllite-1Tc. The computational scheme included a plane-wave basis set along with new pseudopotentials for Si, Al, and O generated using the Perdew−Wang 91 generalized gradient approximation for the core electron exchange-correlation functional, the same approximation that was used for the valence electrons. Our calculations allowed full structural relaxation and, therefore, were appropriate for comparison to ambient-pressure crystallographic data. The simulation results gave an excellent account of bond lengths and angles when compared to single-crystal X-ray diffraction data. Subtle features of the pyrophyllite structure, such as tetrahedral rotation and corrugation of the basal planes, also were captured accurately. The orientation angle of the structural OH groups in pyrophyllite was predicted to be 25.4° relative to the *ab* plane but was found to exist within a very broad minimum in respect to its effect on the total energy of the crystal. Overall we conclude from our results that high-quality DFT optimizations now can provide significant crystallographic information to aid in the interpretation of diffraction and spectroscopic data on layer type aluminosilicates.

I. Introduction

Smectite clay minerals have long presented a significant challenge to experimental crystallography, partly because they cannot be obtained as single crystals and partly because they are believed to exhibit local structural environments not readily amenable to conventional diffraction techniques.[1] In particular, systematic variations in local structure caused by metal cation substitutions in the octahedral and tetrahedral sheets are accessible to experimental study only when diffraction is supplemented by spectroscopic methods.[2−6] Moreover, the orientation of the structural OH groups in smectites remains poorly known because of the invisibility of hydrogen to X-ray diffraction.

In recent years the interpretation of both diffraction and spectroscopic data on clay minerals has been facilitated by a class of independent, first-principles (sometimes termed "ab initio") quantum-mechanical simulations, which now have achieved sufficient accuracy to predict crystallographic properties of clay minerals without recourse to empirical parametrization.[7] The ingredients of this scheme are the atomic nuclei and electrons whose interactions are described by the density functional theory (DFT) formulation of quantum mechanics.[8] DFT-based methods are able to describe structure and bonding properties to a high degree of accuracy, including structural trends.[9−15] Indeed, these methods represent the only practical quantum-mechanical approach for studying complex materials such as layer aluminosilicates while including electron correlation. Admittedly, the approximation to the exchange and correlation energy needed for practical DFT calculations is known to result in a systematic underestimation of bond lengths by 1−2% in the case of the "local density approximation" (LDA) or an overestimation by about 1% for "generalized gradient approximations" (GGAs).[12] This may seem poor performance when compared to experimental crystallographic methods, for which precisions of 1 part in 10 000 are routine. However, an examination of the origin of the underestimation problem reveals it to be mostly a systematic error in calculating the radius of the atomic core. Since core electrons do not participate in bonding and are only weakly perturbed by their local chemical environment, there is good reason to expect that chemical bonding is described with a much greater accuracy than a simple consideration of bond lengths might suggest. Indeed, recent studies of bulk, surface, and defect structures in metals, semiconductors, and insulators (notably minerals) have shown DFT to provide a realistic and accurate description of metallic, ionic, and covalent chemical bonding.[16−19]

In the context of mineral simulations using empirically fitted potentials, it has been observed that a stringent test of simulation results is provided by comparison of bond angles, which are sensitive to angularly dependent covalency effects.[20] However, only a small number of first-principles studies of clay minerals that use the periodic boundary conditions necessary to model crystallographic data are extant in the literature. There is a study of kaolinite with a local basis-set method[7] and a plane-wave pseudopotential study of pyrophyllite.[21,22] Both of these studies

* To whom correspondence should be addressed. E-mail: sungho_park@lbl.gov (S.H.P.); K.Refson@rl.ac.uk (K.R.).

10.1021/jp0347670 CCC: $25.00
Published on Web 11/08/2003

suffered from the limitation that they did not optimize unit cell parameters in response to internal stress. This means that the structural parameters reported were calculated at some undetermined, nonzero pressure. Bond angles are particularly sensitive to pressure because of the relative weakness of the forces involved as compared to bond lengths. Stackhouse et al.[22] performed a DFT calculation on pyrophyllite to obtain an optimized geometry to be used as a template for the 2:1 clay mineral, montmorillonite. However, they did not attempt to converge their simulations with respect to either plane-wave cutoff or Brillouin-zone sampling.

Therefore, to test more conclusively the accuracy of DFT simulations of 2:1 clay mineral systems, we have performed calculations on a mineral for which high-quality crystallographic data are available, namely, pyrophyllite-1Tc.[23] Our calculations allowed full structural relaxation, including lattice parameters, and, therefore, are appropriate for comparison to ambient-pressure crystallographic data. As well as testing methodology, our results provide a reference for further systematic studies of a range of smectites (which are isostructural with pyrophyllite) along a substitutional series of which pyrophyllite is one end member. The present paper gives a detailed prediction of crystal structure parameters and a comparison with experimental results which support the proposition that high-quality DFT studies can indeed provide significant crystallographic information when experimental data may be ambiguous or absent. For pyrophyllite, there remains a notable gap in the available crystallographic data, namely, the position of hydrogen in the structural hydroxyl groups located at the bottom of the ditrigonal cavities in the siloxane surface. We present new DFT simulation results on this as yet unmeasured feature of the pyrophyllite structure.

II. Computational Methods

Structural optimization of pyrophyllite-1Tc was performed using the program CASTEP.[8,24,25] There are a number of implementations of DFT for materials modeling, each offering different levels of accuracy, efficiency, and computational capability. We implemented a variant closely related to the original method of Car and Parrinello[26] based on a plane-wave basis set using pseudopotentials.[8] This is among the most accurate of DFT methods, surpassed only by all-electron FP-LAPW methods.[27] The basis set may be systematically improved to any desired degree of convergence by adjusting the plane-wave cutoff energy and the density of the Mokhorst−Pack grid used for sampling the Brillouin zone. The only remaining approximations are in the pseudopotentials employed and the choice of exchange-correlation functional.

For the latter, we used the Perdew−Wang 91 GGA,[28] which has been tested extensively in studies of oxide minerals.[9,10,19] Of particular importance to the present study, it has been found to give a more accurate description of hydrogenous and hydrogen-bonded systems than the LDA.[29,30] Our pseudopotentials were of the "ultrasoft" variety constructed by the method of Vanderbilt.[31] They require a smaller plane-wave cutoff energy than any other type, and therefore, they yield a lower computational cost, particularly for first-row p elements (e.g., oxygen) and transition metals. They also have a less well known advantage: They are more transferable and accurate than the older norm-conserving type. This is because pseudopotentials are constructed to match the isolated atom orbitals at two distinct energies and include a representation of the charge density from core electrons.

TABLE 1: Computational Details of the Structural Optimizations

simulation	starting configuration	**k** points	grid size	cutoff energy (Ry)
GeOpt 1	WB[a]	2	30 × 30 × 60	29.40
GeOpt 2	GeOpt 1[b]	2	30 × 30 × 60	29.40
GeOpt 3	GeOpt 1_{OH}[c]	2	30 × 30 × 60	29.40
GeOpt 4	WB	16	30 × 30 × 60	29.40
GeOpt 5	WB	2	36 × 36 × 64	36.75

[a] WB = atomic coordinates for a C-centered triclinic cell reported by Wardle and Brindley.[35] [b] Atomic coordinates that were output by simulation GeOpt 1. [c] Same as GeOpt 1, but with only the orientation of the structural OH group relaxed in the simulation.

Two other characteristics of plane-wave methods render them highly suitable for the present study. First, the computer time required scales only as the square of the number of atoms, making it possible to employ simulation cells containing hundreds of atoms. Second, very efficient parallelization schemes and implementations are available,[32] thereby enabling the use of massively parallel supercomputers.

The pseudopotentials we used for Si, Al, and O were generated with the core electrons treated using the same Perdew−Wang 91 GGA as for the valence electrons in contrast to the common practice of generating pseudopotentials using the LDA then using the GGA approximation for valence electrons. Although not strictly erroneous, the inconsistency in the common practice means that the calculation cannot be described by a single, well-characterized exchange-correlation approximation and cannot be compared properly to the results of all-electron computations. Thus, the pseudopotentials we used are highly accurate and well suited for the aluminosilicate modeled.[33]

A plane-wave cutoff energy of 29.40 Ry and Brillouin zone summation over two **k**-points on a 30 × 30 × 60 grid were found sufficient to ensure that the total energy and stress were well converged. Five structural optimizations were performed to explore the effects of starting configuration, structural hydroxyl orientation, number of **k**-points, and cutoff energy (Table 1). Optimizations GeOpt 1 and GeOpt 2 differed by the use of results from an earlier run with only one **k**-point as the starting configuration for the former, whereas output atomic coordinates from GeOpt 1 were the starting configuration for the latter. Optimization GeOpt 3 also began with the GeOpt 2 output atomic coordinates, but only the structural hydroxyl groups were permitted to relax. Optimization GeOpt 4 began as did GeOpt 1 but with many more **k**-points included, and optimization GeOpt 5 involved a plane-wave cutoff energy raised to 36.75 Ry. These last two simulations were designed solely to verify the quality of the choices of **k**-points and cutoff energy in the other optimizations.

III. Results and Discussion

A. Lattice Parameters. Table 2 lists the lattice parameters obtained in optimizations GeOpt 2 (Figure 1), GeOpt 4, and GeOpt 5, together with those reported by Sainz-Diaz et al.[34] and Stackhouse et al.[22] based on simulations and by Wardle and Brindley[35] and Lee and Guggenheim[23] based on X-ray diffraction data. Optimization GeOpt 1 produced negligibly different results from those listed in the table, although its final root mean square stress (0.120 GPa) was somewhat larger than that for GeOpt 2 (0.113 GPa). Both GeOpt 4 and GeOpt 5 produced lattice parameters that deviated from those produced by GeOpt 2 by about 1%, generally in a direction away from the experimental data.

TABLE 2: Calculated and Measured Lattice Parameters for Pyrophyllite-1Tc

				experimental (XRD)		simulations	
	GeOpt 2	GeOpt 4	GeOpt 5	Wardle and Brindley[a]	Lee and Guggenheim[b]	Sainz-Diaz et al.[c]	Stackhouse et al.[d]
a (Å)	5.218	5.239	5.260	5.161(1)	5.160(2)	5.14	5.15
b (Å)	9.079	9.094	9.119	8.958(2)	8.966(3)	9.06	8.93
c (Å)	10.001	9.964	10.106	9.351(2)	9.347(6)	8.14	13.17
α (deg)	90.491	89.732	90.067	91.03(2)	91.18(4)	91.6	90.5
β (deg)	101.727	101.419	101.604	100.37(2)	100.46(4)	101.8	99.2
γ (deg)	89.687	89.558	89.787	89.75(2)	89.64(3)	89.7	89.7
V (Å^3)	463.880	465.300	474.833	425.187(130)	425.157	370.91	597.86

[a] Powder diffraction results.[35] [b] Single-crystal results.[23] [c] Lattice energy minimization results using empirical potentials.[34] [d] DFT results.[22]

TABLE 3: Calculated and Measured Atomic Coordinates for Pyrophyllite-1Tc

	this work[a]			Wardle and Brindley[b]			experimental Lee and Guggenheim[c]		
atom	*x*	*y*	*z*	*x*	*y*	*z*	*x*	*y*	*z*
Al (1)	0.4987	0.1664	−0.0006	0.5000	0.1670	0.0000	0.4995	0.1671	−0.0001
Si (1)	0.7533	−0.0061	0.2794	0.7480	0.0000	0.2890	0.7449	−0.0030	0.2917
Si (2)	0.7709	0.3201	0.2793	0.7590	0.3310	0.2890	0.7595	0.3258	0.2923
O (1)	0.6510	0.0003	0.1115	0.6710	0.0040	0.1130	0.6495	0.0018	0.1155
O (2)	0.7379	0.3034	0.1117	0.7210	0.3190	0.1130	0.7314	0.3079	0.1158
Ob (1)	0.0624	0.3852	0.3437	0.0550	0.3870	0.3530	0.0498	0.3891	0.3589
Ob (2)	0.7394	0.1589	0.3445	0.7240	0.1670	0.3530	0.7251	0.1637	0.3584
Ob (3)	0.5574	0.4381	0.3161	0.5500	0.4480	0.3360	0.5452	0.4426	0.3325
O (OH)	0.2291	0.1905	0.1014	0.2210	0.1860	0.1130	0.2263	0.1927	0.1081
H (OH)	0.1611	0.1073	0.1442	0.148[d]	0.104[d]	0.159[d]	0.1430[d]	0.1107[d]	0.1541[d]

[a] Optimization GeOpt 2. [b] Powder diffraction results.[35] [c] Single-crystal results.[23] [d] H coordinates as calculated by Giese[39] for the Wardle−Brindley structure and then adjusted in the Lee−Guggenheim structure for its systematic deviations from the Wardle−Brindley structure.

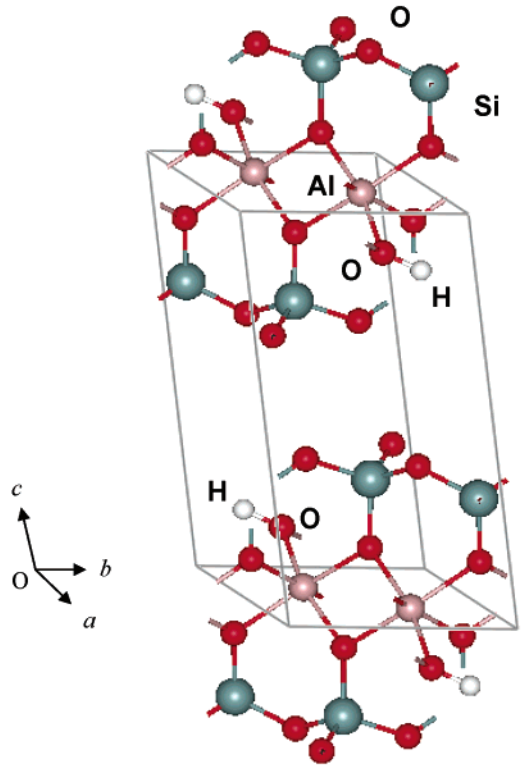

Figure 1. Optimized structure of pyrophyllite (GeOpt 2) $Si_4Al_2O_{10}(OH)_2$: Si (gray); O (red); Al (pink); and H (white).

The tendency in our optimization results is toward a larger unit cell, especially along the *c* dimension, and therefore, a unit cell volume 9% larger than that observed is reported experimentally.[23] A unit cell volume 41% larger than the experimental value was reported by Stackhouse et al.[22] based on their DFT simulation, whereas a simulation using empirical potentials[34] resulted in a unit cell volume 13% smaller than the experimental value. Overall, the lattice parameters produced by GeOpt 2 differ by about 1% from those reported by Lee and Guggenheim.[23] This small difference is apparent also in Table 3, which lists the atomic coordinates calculated in optimization GeOpt 2 along with two sets of experimentally derived values.[23,35]

Table 4 provides details of the interatomic distances and angles within the pyrophyllite structure as calculated in optimization GeOpt 2. As noted by Lee and Guggenheim,[23] the two SiO_4 tetrahedra in pyrophyllite are very similar, as are the Al−O and Al−OH distances. Agreement between calculated and measured interatomic angles is excellent, while that for interatomic distances is good, with an average (positive) deviation of 0.03 Å. On the whole, there is more uniformity in the calculated structure than in the structure determined by single-crystal X-ray diffraction.[23] The systematically longer bond lengths in the calculated structure are typical and characteristic of the use of the GGA.[12]

A projection of the optimized structure along [001] is shown in Figure 2. It compares well with the same projection in Lee and Guggenheim,[23] even to displaying the apparent difference in tilt between Si(1) and Si(2) tetrahedra. A larger-scale view along [001] in Figure 3 shows the offset of the tetrahedral sheets in successive pyrophyllite layers caused by the superposition of the ditrigonal cavities in one basal plane onto oxygens between the cavities in the adjacent layer. This offset stacking arrangement, which distinguishes pyrophyllite from 2:1 clay minerals bearing interlayer cations, is thought to be stabilized by minimization of Si−Si repulsive interactions.[23,36] That it also leads to the deviation of lattice parameters α and *γ* from 90° indicates further, by comparison of these two parameters between optimized and experimental structures (Table 2), that Si−Si repulsion was reasonably well described in our simulations.

TABLE 4: Calculated Interatomic Distances and Angles[a]

Tetrahedra

Si−O bond length (Å)			O−O bond length (tetrahedral edges)			O−Si−O bond angles (deg)		
	Si (1)	Si (2)		Si (1)	Si (2)		Si (1)	Si (2)
Si−O^b	1.63	1.64	O^b−O^b	2.63	2.65	O^b−Si−O^b	107.3	108.1
Si−O^b	1.64	1.63	O^b−O^b	2.70	2.65	O^b−Si−O^b	111.6	108.7
Si−O^b	1.63	1.63	O^b−O^b	2.67	2.70	O^b−Si−O^b	109.3	111.5
Si−O^a	1.66	1.66	O^a−O^b	2.70	2.69	O^a−Si−O^b	109.0	109.2
mean	**1.64**	**1.64**	O^a−O^b	2.68	2.68	O^a−Si−O^b	109.3	109.5
expt	**1.62**	**1.62**	O^a−O^b	2.68	2.69	O^a−Si−O^b	110.3	109.8
			mean	**2.68**	**2.69**	**mean**[a,b]	**109.5**	**109.5**
			expt	**2.64**	**2.64**	**expt**	**109.4**	**109.4**

Octahedron

Al−O (OH) bond length (Å)		O−O length (octahedral edges)		O−Al−O bond angles (deg)	
Al−O	1.95		2.78		94.6
Al−O	1.95		2.79		91.4
Al−O	1.96		2.83		91.9
Al−O	1.94		2.84		92.2
Al−OH	1.91		2.81		91.9
Al−OH	1.91		2.78		95.3
mean	**1.94**		2.89		97.3
expt	**1.91**		2.90		97.7
			3.02		100.9
		mean	**2.85**	**mean**	**94.8**
		expt	**2.81**	**expt**	**94.8**
		(unshared)		(unshared)	
			2.36		76.3
			2.45		78.2
			2.45		77.9
		mean	**2.42**	**mean**	**77.5**
		expt	**2.39**	**expt**	**77.4**
		(shared)		(shared)	
		mean (all)	**2.74**	**mean (all)**	**90.5**

[a] O^b = oxygens in basal plane of the tetrahedral sheet; O^a = apical oxygens; expt = single-crystal X-ray data of Lee and Guggenheim.[23]

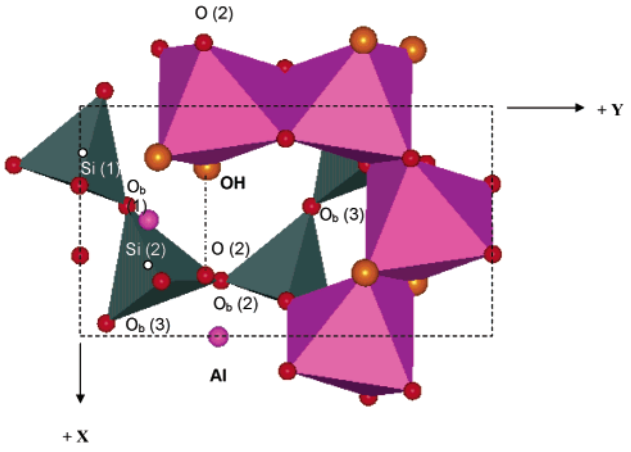

Figure 2. Optimized pyrophyllite (GeOpt 2) unit cell structure projected down along [001]. One tetrahedral sheet is not shown and portions of the octahedral sheet have been deleted to simplify the projection.

B. Structural Distortions. Formation of the 2:1 layer structure in pyrophyllite produces in the component tetrahedral and octahedral sheets distortions of the ideal hexagonal symmetry that are manifest in several ways: (a) rotation of tetrahedra in the (001) plane (T_{rot}) and the resultant decrease in separation between their apical oxygens (AO); (b) thickening of tetrahedra (T_d thickness); (c) flattening of octahedra (octahedral thinning), thus decreasing the mean octahedral angle (ψ); and (d) corrugation of the basal plane oxygens, resulting in a tilt (T_{tilt}) of the bases of tetrahedra bases out of the (001) plane.

These structural parameters were calculated with our simulation results as follows[23,37,38]

$$T_{rot}\,(^\circ) = \frac{1}{2}\,[120^\circ - (\mathrm{O_b{-}O_b{-}O_b\ angle})] \quad (1)$$

$$\mathrm{AO\ (Å)} = \frac{2}{3^{1/2}}\, e_{tet} \cos(T_{rot}) \quad (2)$$

where e_{tet} is the mean tetrahedral edge (O−O) length

$$T_d\ \text{thickness (Å)} = [(\text{mean } z \text{ coordinate of basal O}) - (\text{mean } z \text{ coordinate of apical O})]\ \csc\beta \quad (3)$$

$$\psi\ (\text{deg}) = \cos^{-1}\left(\frac{1}{2}\, O_h \div \text{mean Al−O (OH) distance}\right) \quad (4)$$

where

$$O_h = [(\text{mean } z \text{ coordinate of "upper" O and OH in the octahedral sheet}) - (\text{mean } z \text{ coordinate of "lower" O and OH in the octahedral sheet})]\ \csc\beta \quad (5)$$

is the thickness of the octahedral sheet

$$T_{tilt}\ (\text{deg}) = \text{angle between the planes of two adjacent triangular bases of tetrahedra} \quad (6)$$

$$\Delta Z_{ave}\ (\text{Å}) = \text{corrugation of basal oxygens along [110] which results in the tilt angle between the planes of two adjacent triangular bases of tetrahedra} \quad (7)$$

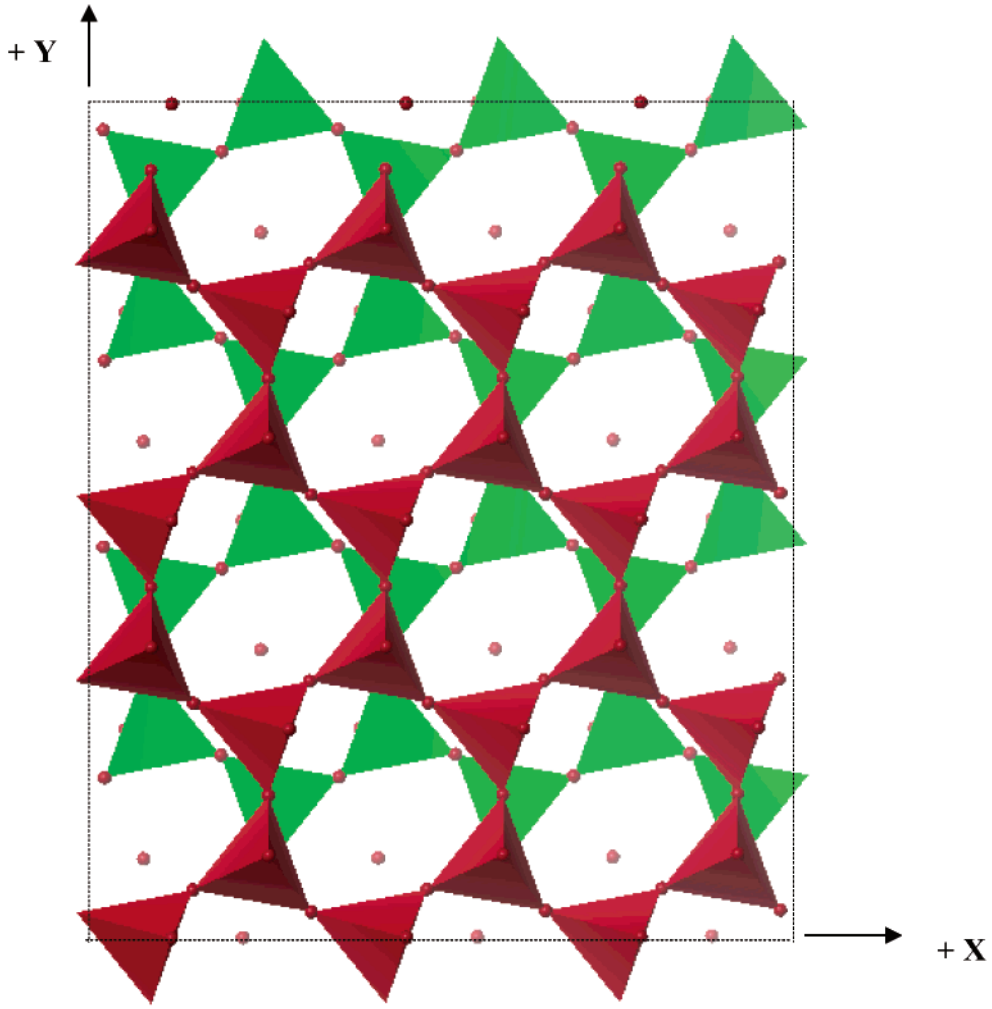

Figure 3. Layer stacking in pyrophyllite as obtained from structural optimization (GeOpt 2). Basal oxygens of one T_d sheet (red) superimpose between the basal oxygens of the hexagonal (ditrigonal) cavities of the T_d sheet in the adjacent layer (green).

TABLE 5: Structural Distortion Parameters for Pyrophyllite-1Tc

	this work	experimental[a]	force field simulation[d]
T_{rot} (deg)[b]	10.07 (0.47)	10.2	8.0
AO (Å)	3.04 (0.03)	3.00	3.03
T_d thickness	2.18 (0.05)	2.153	2.14
ψ (deg)	56.72 (0.03)	57.1	55.2
O_h (Å)	2.126	2.08	2.04
T_{tilt} (deg)[c]	6.7 [6.1]	7.0 [6.0]	
ΔZ_{ave} (Å)	0.212	0.240	0.2

[a] Lee and Guggenheim.[23] [b] Calculated with eq 1 using the mean value of six $O_b-O_b-O_b$ angles (Table 4). [c] Value in brackets is attributed to corrugation, with the remaining tilt angle (0.6°) attributed to the deviation of the mean largest O^a-Si-O^b angle (110.05°, Table 4) from the ideal tetrahedral value, 109.47°. [d] Lattice energy minimization using empirical potentials.[34]

Values of these parameters as found from the GeOpt 2 simulation results are listed in Table 5.

Bonding the tetrahedral sheets to the octahedral sheet through the apical oxygens in the former imposes rotations on the SiO_4 tetrahedra in the basal plane and shortens the distance between the apical oxygens (Figure 4). Lee and Guggenheim[23] report an average $T_{rot} = 10.2°$ and AO = 3.00 Å, the latter parameter being reduced below the ideal hexagonal-arrangement value of 3.05 Å. The corresponding values from optimization GeOpt 2 are 10.1 ± 0.5 and 3.04 ± 0.03 Å, both of which are in agreement with the experimental results. The same is true for the tetrahedral sheet thickness (Table 5).

However, the octahedral angle ψ found by structural optimization is significantly smaller than that reported by Lee and Guggenheim,[23] and therefore, it is closer to the ideal octahedral value, 54.73°. This means that the simulated octahedra are not as flattened, and the octahedral thickness (O_h) is not as diminished, as is observed experimentally. Consequently, the shortened, shared octahedral edges (Table 4) are longer in the optimized structure (2.42 vs 2.39 Å observed experimentally).

The angle of tetrahedral tilt out of the (001) plane is the result of deviation of the O^a-Si-O^b angle (mean value = 110.05° (Table 4)) from the ideal tetrahedral angle (109.47°). Therefore, the contribution to the tilt angle is 0.58° (=110.05° − 109.47°), leaving 6.12° attributed to corrugation. This latter contribution is almost identical to the experimental value (Table 5), while the former contribution is about half as large as the experimental value. It follows that the shift of the apical oxygens parallel to the (001) plane induced by an enlarged tetrahedral angle[23] is less significant in the optimized structure than that observed experimentally. Overall, the results in Table 5 indicate that the optimized structure is somewhat more ideal than the structure

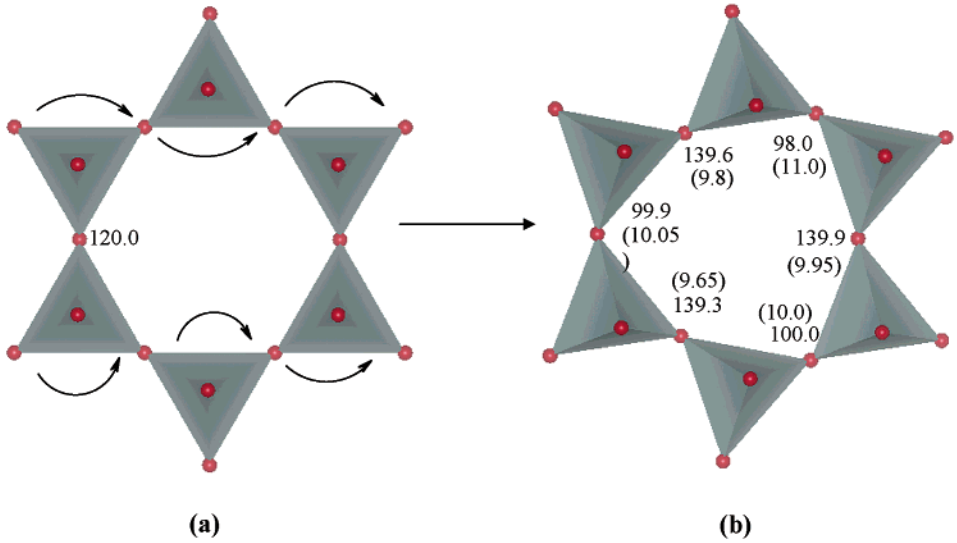

Figure 4. Rotation of SiO_4 tetrahedra (after Rayner and Brown 1966, 1973): (a) ideal hexagonal structure; and (b) optimized structure (GeOpt 2). Rotations of tetrahedrons are denoted by arrows. The resulting $O_b-O_b-O_b$ angles are shown with the rotated tetrahedra. Corresponding values of T_{rot} are in parentheses.

observed in nature. Sainz-Diaz et al.[34] also reported structural distortion parameters for pyrophyllite-1Tc based on their calculations using empirical potentials (Table 5). Their calculated distortion parameters match relatively well with experimental values, except for an underestimated tetrahedral rotation angle (T_{rot}) that our DFT calculation predicted accurately.

C. Structural OH Orientation. The orientation of the structural OH groups in pyrophyllite has not yet been determined experimentally, but molecular modeling estimates are available. Giese[39] used an electrostatic model to calculate an angle of 26° between the OH axis and the *ab* plane, and his estimate was accepted by Lee and Guggenheim.[23] Using a valence force field model, Teppen et al.[40] estimated 0° for this angle (which seems very unlikely) and Bridgeman et al.[41] used an early version of CASTEP to find 22.23°. Stackhouse and co-workers[22] obtained 26 ± 3° for the OH angle with an OH bond length of 0.970 Å from their DFT study. The value predicted by GeOpt 2 is 25.43°, with an OH bond length of 0.974 Å. This result may be compared with 24.72° predicted by GeOpt 1 and 26.28° by GeOpt 3, both of which also yielded OH bond lengths equal to 0.974 Å.

Optimization GeOpt 3 (Table 1) was implemented specifically to examine the sensitivity of our structural calculation in respect to the OH orientation angle. Its resulting total energy value (−429.9214 Ry) was barely different from that achieved by GeOpt 2 (−429.9117 Ry), suggesting, therefore, that the total energy has a broad minimum when considered exclusively as a function of OH orientation angle. This expectation was confirmed by a series of constrained optimizations (Figure 5), which displayed a weak total energy minimum at 26° and angle fluctuations between as low as 14° and as high as 43° corresponding to k_BT of thermal energy at 300 K. Consequently this OH group will undergo large-angle librations of an amplitude of ±15° or more under ambient conditions. We conclude that both the electrostatic[39] and DFT model estimates of the structural OH orientation angle in pyrophyllite are consistent. As noted by Giese,[39] this angle is evidently determined largely by repulsive interactions between the structural OH proton and the Si cations in the tetrahedral sheet.

D. X-ray Diffraction Pattern. Hobbs et al.[7] have noted the utility of simulated diffraction patterns for comparing optimized

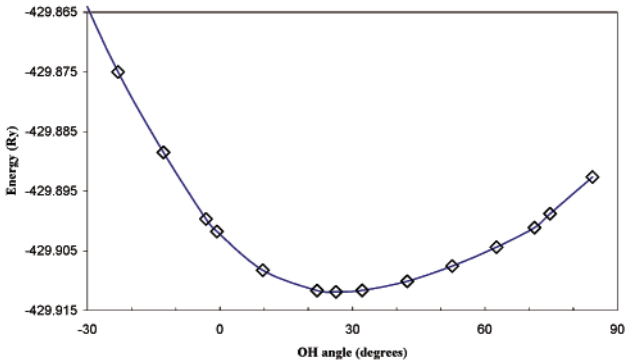

Figure 5. Optimized total energy of pyrophyllite as a function of the out-of-plane OH angle, measured with respect to the *ab* plane. The structural hydroxyl groups were allowed to move freely while all other atoms and structural parameters were fixed (GeOpt 3). A minimum total energy of −429.921 Ry occurs at 26°.

mineral structures with experimentally derived structures. We used the same diffraction software[25] (Cerius2, Accelrys, Inc., San Diego, CA) with an assumed X-ray Cu Kα wavelength (1.541 Å) to calculate the diffraction pattern for optimization GeOpt 2 in the range 0−73° 2θ (Figure 6). Diffraction patterns based on the atomic coordinates given by Wardle and Brindley[35] and Lee and Guggenheim[23] also are shown in Figure 6 (see also Figure 3a in Wardle and Brindley).[35]

The lattice parameters of the two experimentally obtained crystal structures are essentially identical (Table 2), and their atomic coordinates are quite similar (Table 3). Therefore, the powder diffraction patterns calculated for both structures also are quite similar but with certain peak intensities differing by about 10−25%. Since GeOpt 2 has unit cell parameters that are significantly larger than the unit cell parameters reported in the two experimental studies (Table 2), the general profile of most major and minor peaks is comparable to the experimental profiles but with peak positions shifted to lower 2θ. A visual comparison between GeOpt 2 and the structure obtained by Lee and Guggenheim[23] is shown in Figure 7. In the DFT optimization, the sheets are expanded along the *c* axis.

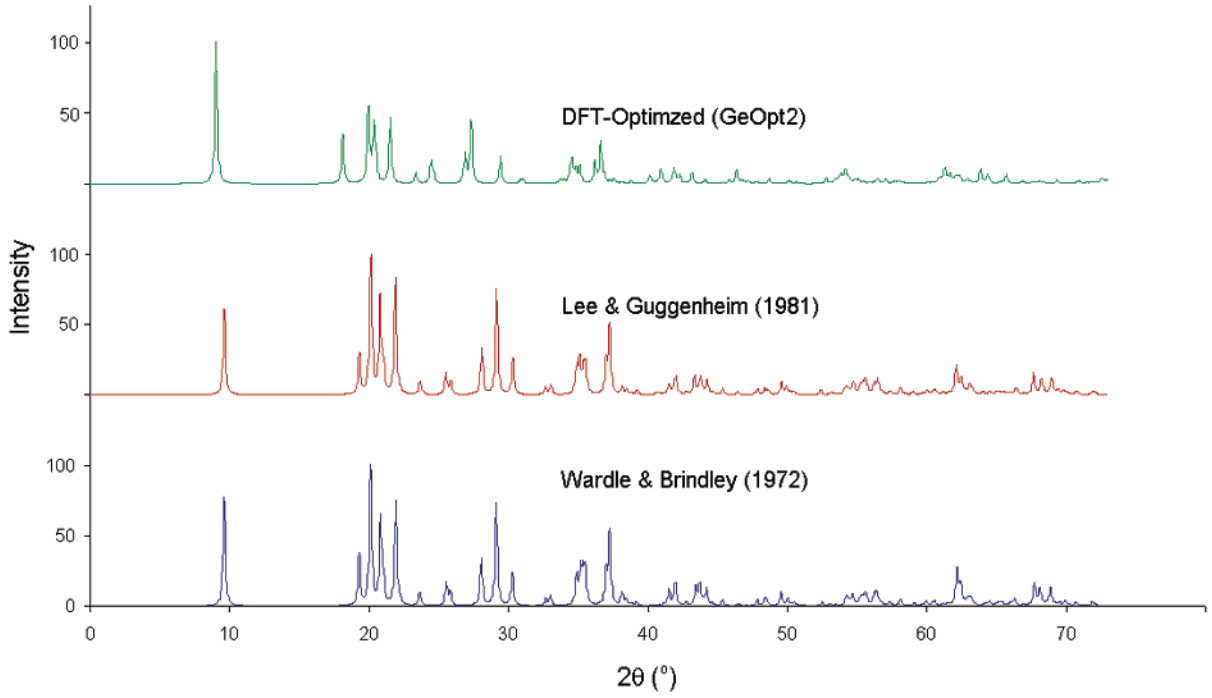

Figure 6. X-ray diffraction patterns of pyrophyllite. The DFT result (GeOpt 2) is compared with diffraction patterns based on the atomic coordinates given by Wardle and Brindley (1972) and Lee and Guggenheim (1981).

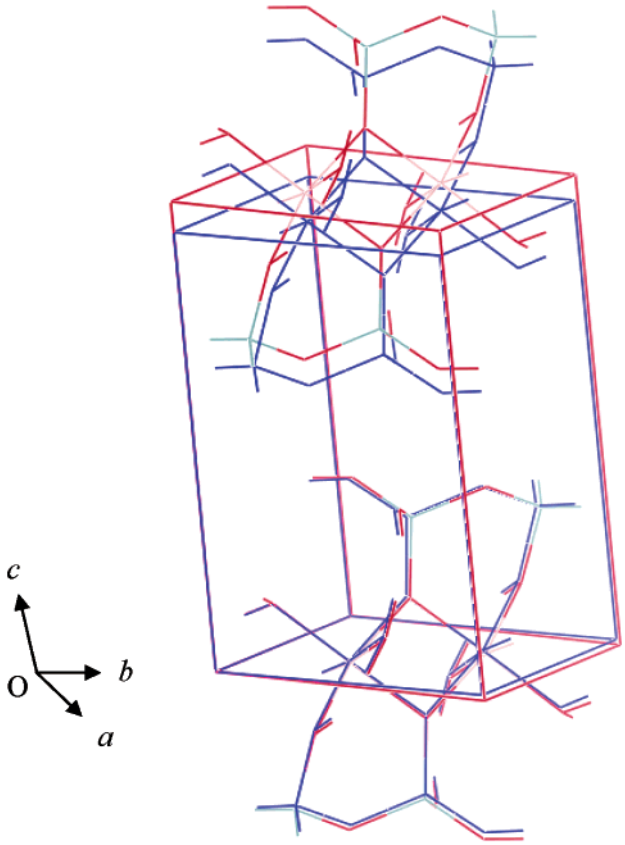

Figure 7. Structural differences between GeOpt 2 and the experimental structure of Lee and Guggenheim (1981). Note that GeOpt 2 (blue) has an expanded cell volume with a longer *c* axis than the experimental structure (unit cell shown in red).

Acknowledgment. The research reported in this paper was supported in part by the Director, Office of Science, Office of Basic Energy Sciences, of the U.S. Department of Energy under Contract No. DE-AC03-76SF00098. The authors express gratitude to the National Energy Research Scientific Computing Center for allocations of time on its Cray T3E and IBM RS/6000 SP supercomputers. We thank Accelrys, Inc., for the use of CASTEP licensed under the Accelrys/UK Car−Parrinello Consortium agreement. The authors also thank Dr. Stephen Guggenheim for helpful comments on the crystallographic data. Gratitude is expressed by the first author to the Environmental Geochemistry Group, Division of Ecosystem Sciences, University of California at Berkeley, for its hospitality during his visit.

References and Notes

(1) Brindley, G. W. Order−disorder in clay mineral structures. In *Crystal Structures of Clay Minerals and Their X-ray identification*; Brindley, G. W., Brown, G., Eds.; Mineralogical Society: London, 1980; pp 125−195.

(2) Decarreau, A.; Grauley, O.; Petit, S. A. *Clay Sci.* **1992**, *7*, 147−167.

(3) Manceau, A.; Chateigner, D.; Gates, W. P. *Phys. Chem. Miner.* **1998**, *25*, 347−365.

(4) Manceau, A.; Lanson, B.; Drits, V. A.; Chateigner, D.; Gates, W. P.; Wu, J.; Huo, D.; Stucki, J. W. *Am. Mineral.* **2000**, *85*, 133−152.

(5) Fumagalli, P.; Stixrude, L.; Poli, S.; Snyder, D. *Earth Planet. Sci. Lett.* **2001**, *186*, 125−141.

(6) Sainz-Diaz, C. I.; Cuadros, J.; Hernandez-Laguna, A. *Phys. Chem. Miner.* **2001**, *28*, 445−454.

(7) Hobbs, J. D.; Cygan, R. T.; Nagy, K. L.; Schultz, P. A.; Sears, M. P. *Am. Mineral.* **1997**, *82*, 657−662.

(8) Payne, M. C.; Teter, M. P.; Allan, D. C.; Arias, T. A.; Joannopoulos. *Rev. Mod. Phys.* **1992**, *64*, 1045−1097.

(9) Winkler, B.; Milman, V.; Hennion, B.; Payne, M. C.; Lee, M. H.; Lin, J. S. *Phys. Chem. Miner.* **1995**, *22*, 461−467.

(10) Winkler, B.; Milman, V.; Payne, M. C. *Mineral. Mag.* **1995**, *59*, 589−596.

(11) Kenny, S. D.; Desmond, J.; McConnell, C.; Refson, K. *Am. Mineral.* **2000**, *84*, 1681−1685.

(12) Gale, J. D.; Rohl, A. L.; Milman, V.; Warren, M. C. *J. Phys. Chem. B* **2001**, *105*, 10236−10242.

(13) Benco, L.; Tunega, D.; Hafner, J.; Lischka, H. *J. Phys. Chem. B* **2001**, *105*, 10812−10817.

(14) Benco, L.; Tunega, D.; Hafner, J.; Lischka, H. *Am. Mineral.* **2001**, *86*, 1057−1065.

(15) Benco, L.; Tunega, D.; Hafner, J.; Lischka, H. *Chem. Phys. Lett.* **2001**, *333*, 479−484.

(16) Deyirmenjian, V. B.; Heine, V.; Payne, M. C.; Milman, V.; Finnis, M. W. *Philos. Mag. Lett.* **1996**, *73*, 39−44.
(17) Christensen, A.; Carter, E. A. *Phys. Rev. B* **1998**, *58*, 8050−8064.
(18) Yildirim, T.; Gülseren, O.; Kiliç, Ç; Ciraci, S. *Phys. Rev. B* **2000**, *62*, 12648−12651.
(19) Brodholt, J. P.; Refson, K. *J. Geophys. Res., [Solid Earth]* **2000**, *105*, 18977−18982.
(20) Purton, J. A.; Bird, D. M.; Parker, S. C.; Bullett, D. W. *J. Chem. Phys.* **1999**, *110*, 8090−8097.
(21) Chatterjee, A.; Iwasaki, T.; Ebina, T. *J. Phys. Chem. A* **2000**, *104*, 8216−8223.
(22) Stackhouse, S.; Coveney, P. V.; Sandre, E. *J. Am. Chem. Soc.* **2001**, *123*, 11764−11774.
(23) Lee, J. H.; Guggenheim, S. *Am. Mineral.* **1981**, *66*, 350−357.
(24) Teter, M. P.; Payne, M. C.; Allan, D. C. *Phys. Rev. B* **1989**, *40*, 12255−12263.
(25) Accelrys *Cerius2 Molecular Simulation Software*, version 4.2; Material Science, Accelrys: San Diego, CA, 2001.
(26) Car, R.; Parrinello, M. *Phys. Rev. Lett.* **1985**, *55*, 2471−2474.
(27) Wei, S.-H.; Krakauer, H. *Phys. Rev. Lett.* **1985**, *55*, 1200−1203.
(28) Perdew, J. P.; Wang, Y. *Phys. Rev. B* **1992**, *45*, 13244−13249.
(29) Perdew, J. P.; Burke, K. *Int. J. Quantum Chem.* **1996**, *57*, 309−319.
(30) Sprik, M.; Hutter, J.; Parrinello, M. *J. Chem. Phys.* **1996**, *105*, 1142−1152.
(31) Vanderbilt, D. *Phys. Rev. B* **1990**, *41*, 7892−7895.
(32) Clarke, L. J.; Stich, I.; Payne, M. C. *Comput. Phys. Commun.* **1992**, *72*, 14−28.
(33) Civalleri, B.; Harrison, N. M. *Mol. Simul.* **2002**, *28*, 213−237.
(34) Sainz-Diaz, C. I.; Hernandez-Laguna, A.; Dove, M. T. *Phys. Chem. Miner.* **2001**, *28*, 130−141.
(35) Wardle, R.; Brindley, G. W. *Am. Mineral.* **1972**, *57*, 732−750.
(36) Zvyagin, B. B.; Mishchenko, K. S.; Soboleva, S. V. *Soviet Physics, Crystallography* **1969**, *13*, 511−515.
(37) Guggenheim, S. The brittle micas. In *Reviews in Mineralogy*; Bailey, S. W., Ed.; Mineralogical Society of America; Washington, DC, 1984; Vol. 13, pp 61−104.
(38) Guggenheim, S. Personal communication.
(39) Giese, R. F. *Nature, Phys. Sci.* **1973**, *241*, 151.
(40) Teppen, B. J.; K., R.; Bertsch, P. M.; Miller, D. M.; Schäfer. *J. Phys. Chem. B* **1997**, *101*, 1579−1587.
(41) Bridgeman, C. H.; Buckingham, A. D.; Skipper, N. T.; Payne, M. C. *Mol. Phys.* **1996**, *89*, 879−888.